博士論文

Development of multiple pathway-specific gene transfer methods

based on the host specificity of avian sarcoma leukosis virus.

（鶏肉腫白血病ウイルスの宿主特異性に基づいた多経路選択

的遺伝子導入法の開発）

松山　真

Contents

Abstract

Pathway-specific gene delivery is requisite for understanding complex neuronal systems in which neurons that project to different target regions are locally intermingled. However, conventional genetic tools cannot achieve simultaneous, independent gene delivery into multiple target cells with high efficiency and low cross-reactivity. In this study, I systematically screened all receptor–envelope pairs resulting from the combination of four avian sarcoma leukosis virus (ASLV) envelopes (EnvA, EnvB, EnvC, and EnvE) and five engineered avian-derived receptors (TVA950, TVB^{S3}, TVC, TVB^T, and DR-46TVB) *in vitro*. Four of the twenty pairs exhibited both high infection rates [TVA–EnvA, 99.6%; TVB^{S3}–EnvB, 97.7%; TVC–EnvC, 98.2%; and DR-46TVB–EnvE, 98.8%] and low cross-reactivity ($< 2.5\%$). Next, I tested these four receptor-envelope pairs *in vivo* in a pathway-specific gene-transfer method. Neurons projecting into a limited somatosensory area were labeled with each receptor by retrograde gene transfer. Three of the four pairs exhibited selective transduction into thalamocortical neurons expressing the paired receptor (>98%), with no observed cross-reaction. Finally, by expressing three receptor types in a single animal, I achieved pathway-specific, differential fluorescent labeling of three thalamic neuronal populations, each projecting into different somatosensory areas. Thus, I identified three orthogonal pairs from the list of ASLV subgroups and established a new vector system that provides a simultaneous, independent, and highly specific genetic tool for transferring genes into multiple target cells *in vivo*. Our approach is broadly applicable to pathway-specific labeling and functional analysis of diverse neuronal systems. (239 words)

Introduction

In the mammalian brain, neurons projecting to different target regions are locally intermingled, and even adjacent neurons can have different connectivities and functions (1-5). To disentangle such complex networks, anatomical mapping and individual manipulation of each neural pathway are both critical. To date, conventional genetic tools, such as site-specific recombinase (Cre/loxP) (6), prokaryotic DNA binding protein (Tet-On/Off system) (7), and a viral receptor–envelope pair (TVA–EnvA) (8) have been used to genetically control specific neural pathways in the mammalian brain, usually in combination with retrograde viral infection (9).

Despite their usefulness, these technologies can simultaneously manipulate no more than two neural pathways, a number that is far from sufficient for a dissection of natural brain circuitry. For example, the thalamus is a relay station that receives almost all sensory information and sends motor signals to the diverse cortical areas (10). In order to fully understand this integration of multisensory inputs and the distribution of appropriate motor outputs, so many pathway-specific neuronal populations need to be monitored and manipulated, both individually and simultaneously. In addition, the simultaneous dissection of each pathway in a single animal is important in experiments using non-human primates because unlike the use of rodents, the associated high costs in time, money, and effort make using multiple non-human primates unfeasible. Therefore, it is necessary to increase the number of available tools. One challenge to doing so is that all such tools need to be

orthogonal; in other words, the biological reactions on which they are based must not cross-react.

A number of biochemical mechanisms are potentially applicable to orthogonal gene expression systems. One of the most promising candidates is the use of specific combinations of virus envelope proteins (Env) and corresponding receptors. Because viral vectors pseudotyped with Env exclusively infect cells that express compatible receptors, exogenous expression of receptors in target cells provides a specific guide for viral entry. However, some viruses can use more than one molecular species as receptors, and these receptors provide a variety of functions essential for viral entry. In simple situations, receptors bind to virus envelopes and initiate endocytic uptake of viruses; alternatively, receptors affect cellular signaling pathways which facilitate virus entry, or they directly activate fusion/penetration processes by inducing conformational changes in Env proteins (11).

Among the enveloped viruses, I focused on avian sarcoma leukosis virus subgroups (ASLVs) for three reasons. First, ASLVs' natural host range is restricted to birds. Therefore, it is likely that ASLV-pseudotyped viral vectors will exhibit low nonspecific infectivity toward mammalian neurons via endogenous receptors. Second, ASLVs are reported to require single molecular species as receptors, and this simple mode of infection is suitable for adaptation as a conditional gene-delivery system. Third, many different Env and receptor proteins are available from among six distinct ASLV subgroups (A, B, C, D, E, and J) and ten different receptors (12), and there is evidence that some ASLV Env proteins

exhibit specific binding to disparate receptor sequences. For example, chicken TVA protein belongs to the family of low-density lipoprotein receptors and determines susceptibility to ASLV-A (13). The tumor necrosis factor receptor-related proteins TVB[S1] and TVB[S3] confer susceptibility to ASLV-B/-D/-E, and ASLV-B/-D, respectively (14). ASLV-C utilizes the TVC protein of the butyrophilin family, which contains two immunoglobulin-like domains (15). TVB[T], a turkey homolog of TVB, is an ASLV-E–specific receptor (16). Finally, ASLV-J uses the chicken multi–membrane-spanning cell-surface protein Na^+/H^+ exchanger type 1 (chNHE1) as a receptor (17).

However, no study to date has systematically and quantitatively determined which types of ASLVs can infect with high efficiency mammalian cells expressing a single receptor, nor has any study shown which combination of envelopes and receptors of ASLV specifically interact with each other. In this study, I first performed *in vitro* and *in vivo* screens to identify orthogonal receptor–envelope pairs. I then conducted a proof-of-concept study *in vivo* to demonstrate that these orthogonal pairs can achieve pathway-specific differential fluorescent labeling of multiple neuronal populations, each projecting to different cortical regions. Our findings expand the repertoire of genetic tools that can be used to dissect and manipulate the complex neural networks created by intermingled neurons projecting to different target regions. (687 words)

Results

Putative orthogonal ASLV receptor–envelope pairs

The various ASLV subgroups exhibit different infectious properties in chicken cell lines (CEFs and DF-1 cells) (13-18). Based on these data, I estimated the feasibility of six envelopes and seven receptors as genetic tools, and eliminated several (TVB^{S1}, ASLV-D envelope, ASLV-J envelope, and chNHE1) for the following reasons: TVB^{S1} is a nonspecific cellular receptor for ASLV-B, -D, and -E (14, 18); ASLV-D can infect a variety of mammalian cell lines in the absence of exogenous receptors (19-21); and chNHE1, the receptor for ASLV-J (17), may alter neuronal membrane potential. Additionally, I selected TVA950, a transmembrane form, from two splice-variant forms of TVA, even though the other form of TVA (TVA800, a chicken glycophosphatidylinositol (GPI)-anchored form) has been used in previous studies (8, 22, 23). I chose the transmembrane form because GPI-anchored proteins contain a signal peptide in the C-terminus that is cleaved off and replaced by the GPI-anchor, precluding the use of C-terminal epitope tags. This process narrowed down the set of candidates to four receptors (TVA950, TVB^{S3}, TVC, and TVB^{T}) and four envelopes (EnvA, EnvB, EnvC, and EnvE) (Fig. 1A).

Measurement of orthogonality between the receptor–envelope pairs *in vitro*

To examine the orthogonality of the receptor–envelope pairs, I tested the various combinations to determine which ones afforded specific viral entry and transgene expression in human embryonic kidney (HEK) 293T cells. To mitigate the unwanted side effects associated with the expression of an exogenous transmembrane protein in mammalian cells, I deleted the original intracellular domains from each receptor (Fig. 1B). Epitope tags (HA, c-Myc, V5, and 3×FLAG) were C-terminally fused to the receptors to allow detection by immunohistochemistry. To increase protein half-life according to the mammalian N-end rule (24), the N-termini of the receptors were also modified, such that valine was the second amino acid.

I then developed two types of recombinant lentiviral vectors: FuGB2-pseudotyped bicistronic vectors that co-expressed the engineered receptor and *Aequorea coerulescens* green fluorescent protein (AcGFP1) and ASLV Env-pseudotyped vectors that expressed mCherry (Fig. 2A). The FuGB2-pseudotyped lentiviral vector, which can transduce dividing and non-dividing cells, is suitable for use in both *in vitro* and *in vivo* assays. The cytomegalovirus (CMV) promoter was selected because it drives a high level of protein expression in the mammalian brain (25) and has been used previously for TVA expression (8, 22, 23, 26). I tested all possible receptor–envelope combinations by serially infecting receptor-expressing and Env-pseudotyped vectors into HEK 293T cells. mCherry expression was observed in only five pairs: TVA950–EnvA, TVB[S3]–EnvB, TVC-EnvC, TVB[T]-EnvB, and TVB[T]-EnvE (Figs. 2B–E). Although the results obtained with TVA950–EnvA, TVB[S3]–EnvB, and TVC-EnvC were consistent with those obtained in DF-1 cells,

the infection of EnvB vector into TVB^T-expressing cells observed in our assays was inconsistent with previous reports.

I next sought to rationally design an alternative EnvE-specific receptor for TVB^T. The chimeric protein DR-46TVB was engineered by exchanging the first cysteine-rich domain of chicken TVB^{S1}, which is critical for ASLV-B infection (27), with those of the human TVB homolog DEATH RECEPTOR 5. HEK 293T cells expressing this chimeric receptor expressed mCherry in combination with EnvE vector, but not EnvB vector (Fig. 2F).

These results were quantitatively confirmed by flow cytometry. A progressive shift to the right was observed only in the histograms for the following six pairs: TVA950–EnvA, TVB^{S3}–EnvB, TVC–EnvC, TVB^T–EnvB, TVB^T–EnvE, and DR–46TVB-EnvE (Fig. 3A). Furthermore, the infection rates (the ratio of AcGFP1/mCherry double-positive cells to all AcGFP1-positive cells under each condition) for TVA950–EnvA, TVB^{S3}–EnvB, TVC–EnvC, and DR-46TVB–EnvE were significantly higher than those of the other pairs (one-way analysis of variance [ANOVA] and Scheffe's F-test, $P < 0.001$) except for TVB^T–EnvB and TVB^T–EnvE (Fig. 3B and Table S1). Together, these data demonstrate that these four pairs (TVA950–EnvA, TVB^{S3}–EnvB, TVC-EnvC, and DR-46TVB–EnvE) are orthogonal in HEK 293T cells.

Orthogonality of the TVA950–EnvA pair *in vivo*

Having demonstrated that the four aforementioned orthogonal pairs were capable of transferring genes into cultured mammalian cells, I next examined the gene transfer capability and the orthogonality of our receptors and envelopes *in vivo* using the thalamocortical system of rats. In a pilot study, I injected FuGB2-TVC vector along with a mixture of EnvA/EnvB/EnvC/EnvE vectors into five rats. I did not observe any sign of infection by the EnvC vector in these rats *in vivo* (data not shown). Hence, the TVC–EnvC pair was not used in the following experiment.

I first tested the specificity of the TVA950–EnvA pair (Fig. 4A). In these experiments, the retrograde vector expressing TVA950 (FuGB2–TVA950) was injected into the primary somatosensory cortex (S1) (Fig. 4B), and a mixture of EnvA/EnvB/EnvE vectors that expressed different fluorescent proteins (XFPs) was injected into the thalamus (EnvA vector expressing blue fluorescent protein [BFP], EnvB vector expressing enhanced green fluorescent protein [EGFP], and EnvE vector expressing tdTomato). In sections immediate vicinity of either the FuGB2-TVA950 or Env vectors' injection site, many BFP-positive axons in S1 or cells in the thalamus were observed, respectively (Fig. 4C). Near the FuGB2–TVA950 vector injection site, dense projections of BFP-positive axons were observed in layers I, IV, and VI (Fig. 4D), consistent with the projection pattern of thalamocortical neurons (28-32). By contrast, around the injection sites of the Env vectors, BFP-positive cells were detected in the ventral posteromedial thalamic nucleus (VPM) and the posteromedian thalamic nucleus (POm) (Fig. 4E); all BFP-positive cells were neurons, as evidenced by double labeling with an anti-NeuN antibody (Fig. 4F). Next, I compared the distribution of TVA950-positive neurons with that of the BFP-positive neurons in brain

sections, using an anti-HA antibody to immunohistochemically detect the HA-tagged TVA950 protein. Notably, BFP expression was observed only in these thalamic neurons, even though HA-tagged TVA950 protein expression was also observed in cortices with neurons projecting to the injection site of the TVA950-expressing vector, indicating that our vector system selectively visualized a single pathway (Fig. S1A).

A quantitative analysis performed using sections stained for the HA epitope tag revealed that more than 99% of BFP-positive neurons were TVA950-positive (ratio of BFP and TVA950 double-positive neurons to all BFP-positive neurons: 1942/1959) (Fig. 4G), whereas none were EGFP- or tdTomato-positive neurons (Fig. 4H). Similar results were observed for the other two rats (974/982 and 572/580, Table 1), showing that the EnvA vector leads to specific transduction of TVA950-positive neurons and other EnvB/EnvE vectors do not transduce TVA950-positive or –negative neurons *in vivo*.

Orthogonality of the TVB^{S3}–EnvB pair *in vivo*

I also tested the specificity of the TVB^{S3}–EnvB pair *in vivo* (Fig. 5A). In this experiment, I injected FuGB2-TVB^{S3} vector into the S1 region, and a mixture of EnvA/EnvB/EnvE vectors into the thalamus (Fig. 5B). The injection coordinates for the FuGB2–TVB^{S3} vector were 2.5 mm posterior to those used for the FuGB2–TVA950 vector in the rats shown in Figure 4. I observed many EGFP-positive axons from thalamic neurons innervating the S1 cortex (Fig. 5C). The EGFP-positive axons projected into cortical layers I, IV, and VI in the S1 cortex near the FuGB2–TVB^{S3} vector injection site (Fig. 5D). To compare the distribution of TVB^{S3}-positive cells with that of EGFP-positive cells, I performed an

11

immunohistochemical analysis using an anti–c-Myc antibody to detect the c-Myc-tagged TVB^{S3} protein in brain sections; EGFP-positive cells were detected only in the VPM and POm (Fig. 5E).

I then performed a quantitative immunohistochemical analysis using the c-Myc epitope tag, and found that 96.7% of EGFP-positive neurons were also TVB^{S3}-positive (ratio of EGFP and TVB^{S3} double-positive neurons to all EGFP-positive neurons: 397/410) (Fig. 5F). By contrast, neither BFP- nor tdTomato-positive neurons were observed (Fig. 5G). Similar results were obtained from the other two rats (1212/1224 and 964/974, Table 1). These results confirmed that the EnvB vector leads to specific transduction of TVB^{S3}-positive neurons and other EnvA/EnvE vectors do not transduce TVB^{S3}-positive or – negative neurons *in vivo*.

Orthogonality of the DR-46TVB–EnvE pair *in vivo*

I next tested the specificity of the DR-46TVB–EnvE pair *in vivo* (Fig. 6A). In these experiments, FuGB2-DR-46TVB vector was injected into the S1 region, and a mixture of EnvA/EnvB/EnvE vectors was injected into the thalamus (Fig. 6B). The injection coordinates for the FuGB2–TVC vector in the rats were 2.5 mm posterior to those used for the FuGB2-TVB^{S3} vector in the rats shown in Figure 5. I observed many tdTomato-positive axons from thalamic neurons innervating the S1 cortex (Fig. 6C). Many tdTomato-positive axons projected into S1 cortical layers I, IV, and VI near the FuGB2–DR46-TVB vector injection site (Fig. 6D). To compare the distribution of the DR-46TVB-positive cells with that of tdTomato-positive cells in brain sections, I performed an immunohistochemical

analysis using an anti-FLAG antibody to detect the 3×FLAG-tagged DR-46TVB protein. The tdTomato-positive cells were detected only in the VPM and POm (Fig. 6E).

I then performed a quantitative analysis using immunohistochemistry with the 3×FLAG epitope tag and found that 99.9% of tdTomato-positive neurons were also DR-46TVB–positive (ratio of tdTomato and DR-46TVB double-positive neurons to all tdTomato-positive neurons: 502/503) (Fig. 6F), whereas none were BFP- or EGFP-positive (Fig. 6G). Among three rats, the average specificity of the DR-46TVB–EnvE pair was 99.7%, the highest among all three receptor–envelope pairs (vs. 99.1% for TVA950–EnvA and 98.7% for TVB^{S3}–EnvB; Table 1). These results confirmed that the EnvE vector leads to the specific transduction of DR-46TVB–positive neurons and other EnvA/EnvB vectors do not transduce DR-46TVB-positive or –negative neurons *in vivo*.

Simultaneous gene transfer in cultured mammalian cells

I next examined whether these three receptor–envelope pairs could be used simultaneously to deliver three different genes into three different cell populations in a single culture. For this purpose, I infected a mixture of EnvA/EnvB/EnvE vectors, each expressing different fluorescent proteins, into an intermingled population of HEK 293T cells in which each cell expressed one of the three receptor proteins (TVA950, TVB^{S3}, or DR-46TVB) (Fig. 7A). The infected cells expressed only one of the three fluorescent proteins in a mutually exclusive manner, creating a three-color cellular mosaic (Fig. 7B). This result confirmed that the infection specificity of the three receptor–envelope pairs is preserved even in the presence of non-optimal receptors and Env vectors *in vitro*.

ASLV receptor–envelope pairs enable triple pathway-specific gene transfer *in vivo*

To demonstrate the selective and simultaneous labeling of three neuronal populations, each projecting to different target regions, I injected three types of receptor-expressing vectors into the different cortical areas in S1 and a mixture of Env vectors into the thalamus (Figs. 8A and 8B). The injection coordinates for each receptor-expressing vector were the same as those shown in Figures 4, 5, and 6. In a confocal tiling of a sagittal section, I distinguished three XFPs in different axons (Fig. 8C). BFP-, EGFP-, and tdTomato-positive axons innervated areas near each injection site. In the thalamus, neurons positive for all three types of fluorescence were present. Although the three Env vectors were injected at the same coordinates, the three types of XFP-positive neurons exhibited different distributions in the thalamus (Fig. 8D). Most of the BFP-positive neurons were medial to the EGFP-positive neurons in the thalamus, and the EGFP-positive neurons were more medial than the tdTomato-positive neurons. Furthermore, individual neurons distinctly expressed BFP, EGFP, or tdTomato in a mutually exclusive manner (Figs. 8E and 8F).

In conclusion, I identified three ASLV receptor–envelope pairs that are orthogonal in mammalian cells and rat brains. These pairs could be used simultaneously in single cultures or individual rats to fluorescently label three distinct subgroups of neurons.

Discussion

By experimentally identifying and characterizing ASLV receptor–envelope pairs in mammalian cells, I engineered a novel multi-targeted gene-transfer system and conducted a proof-of-concept study demonstrating that this system can genetically dissect intermingled neural connections in rat brains (33). The high orthogonality of three artificial ASLV receptors and their corresponding ASLV envelopes was key to the success of this system, and permitted the ASLV-pseudotyped lentiviral vectors to selectively transduce mammalian cells expressing specific receptors *in vitro* and *in vivo*.

I combined highly efficient retrograde gene transfer (HiRet) (34) with our receptor–envelope system to identify neural populations projecting to a target region in the brain. This retrograde system utilizes a mutant rabies virus glycoprotein (FuGB2), in which the cytoplasmic domain of rabies virus glycoprotein has been replaced with the corresponding part of the vesicular stomatitis virus glycoprotein. In this study, HiRet transferred TVA950/TVB^{S3}/DR-46TVB protein genes into not only thalamocortical neurons (Figs. 4F, 5F, and 6F) but also corticocortical neurons (Fig. S1A–C) projecting to the HiRet injection sites. In combination with our receptor–envelope system, each fluorescent protein gene was expressed only in thalamocortical neurons. Our system can also be combined with other retrograde gene-transfer methods, such as NeuRet (35) and recombinant rabies virus (5, 26, 36-39). However, ASLV pseudotyping may change the pH tolerance and stability of viral particles (40-42); consequently, the infectious titer of viral vectors should be checked before use.

ASLVs are divided into six viral subgroups, designated A–E and J, based on their cellular receptors (43). From these ASLV subgroups and receptors, I screened for specificity and efficiency using HEK 293T cells and rat brains. In our *in vitro* assays, the infection rate of TVB^T–EnvB pair was lower than that of TVB^T–EnvE pair but much higher than that of control (Fig. 3). However, TVB^T is reported to permit entry of retroviral vector pseudotyped with EnvE but not EnvB (16). Because I used EnvB-pseudotyped lentiviral vectors at high MOI (MOI=100), weak receptor-envelope interaction was perhaps detected in our experimental condition. With the TVC–EnvC pair, no infection of EnvC vector was observed *in vivo* contrary to our expectations; the reason for this negative result remains unclear. Some viruses, such as human immunodeficiency virus and hepatitis C virus, use multiple cell-surface components to enter host cells (11). Hence, I speculate that ASLV(C)-pseudotyped lentiviral vectors might require factors other than TVC that are present in the HEK 293T cells but not in rat neurons.

One advantage of this receptor-envelope system is its compatibility with other genetic tools. Combining the Cre/loxP and Tet system (6, 7) with the receptor–envelope system allows modifiers of neural activity, such as channelrhodopsin-2 (44, 45), tetanus toxin (46-48), allatostatin (49) and immunotoxin (50, 51), to be selectively introduced and expressed in a more limited population of cell types. In addition, the combination of new optogenetic tools activated by different light wavelengths (52, 53) with the receptor–envelope system may allow the manipulation of each connection separately and simultaneously. Therefore, when combined with other emerging technologies, the system I

describe here should make a powerful contribution to the functional analysis of multiple

neural populations *in vivo*.

Materials and Methods

All experiments were conducted in accordance with the National Institutes of Health (Bethesda, MD, USA) *Guide for the Care and Use of Laboratory Animals* and were approved by the Institutional Review Committee of the University of Tokyo School of Medicine (Tokyo, Japan).

Design of Vector Constructs

The sequences for naive and synthetic receptors (TVA950, TVB^{S3}, TVC, TVB^{T}, and DR-46TVB) for ASLV subgroups were as follows.

TVA950: TVA, consisting of the long form splice variant TVA950 from chicken line H6 and the HA epitope tag, was obtained from plasmid pTVA950(H6) (11). This sequence was subcloned into the lentiviral transfer vector containing the CMV promoter (25), and then subcloned into a bicistronic lentiviral transfer vector that co-expressed a green fluorescent protein (AcGFP1) and a receptor protein mediated by the picornaviral 2A peptide (P2A) under the control of the CMV promoter (54).

TVB^{S3}: TVB^{S3} consisted of TVB^{S3} ΔDD (amino acids 1–280) and a c-Myc epitope tag. TVB proteins contain a putative cytoplasmic death domain (DD), which promotes cell death following envelope–receptor interaction (55, 14). TVB^{S1}, a chicken receptor for the ASLV subgroups B, D, and E, differs from TVB^{S3} exclusively at residue 62 (18). The TVB^{S1} fragment was obtained from the pHA1 plasmid (55), and cysteine 62 was converted to serine, which converted the TVB^{S1} fragment into the TVB^{S3} fragment (18). The c-Myc

18

epitope tag was fused to the C-terminus, and the resulting fragment was subcloned into the lentiviral transfer vector and the bicistronic lentiviral transfer vector.

TVC: TVC consisted of the chicken line H6 TVC protein (amino acids 1–488) and a V5 epitope tag. TVC sequence was obtained from plasmid pTVC-F (15). The V5 epitope tag was fused to the C-terminus, and the resulting fragment was subcloned into the lentiviral transfer vector and the bicistronic lentiviral transfer vector.

TVB^T: TVB^T consisted of $TVB^T\Delta DD$ (amino acids 1–281) and a Flag epitope tag. TVBT sequence was obtained from plasmid TEF24ΔDD (16). The FLAG epitope tag was fused to the C-terminus, and the resulting fragment was subcloned into the lentiviral transfer vector and the bicistronic lentiviral transfer vector.

DR-46TVB: DR-46TVB consisted of DR5 (amino acids 1–80), TVB^{S1} (amino acids 46–280), and a FLAG epitope tag (27). The DR5 sequences were isolated from the HEK 293T cDNA library by PCR. TVB^{S1} (amino acids 1–45) was exchanged for DR5 (amino acids 1–80), and the FLAG epitope tag was fused to the C-terminus. The fragment was subcloned into the lentiviral transfer vector and the bicistronic lentiviral transfer vector.

In this study, lentiviral vectors expressing fluorescent proteins were pseudotyped using the ASLV envelopes EnvA/VSVG, EnvB, EnvC, and EnvE, respectively. Fragments of fluorescent proteins were subcloned into lentiviral transfer vectors containing the CMV promoter. The BFP fragment was obtained from pTagBFP-N (Evrogen, Moscow, Russia), the AcGFP1 fragment from pIRES2-AcGFP1, the mCherry fragment from pmCherry-N1, and the tdTomato fragment from pCMV-tdTomato (all from Clontech Laboratories, Mountain View, CA, USA).

Cell Culture

Human embryonic kidney (HEK) 293T cells were obtained from the RIKEN BioResource Center (Tsukuba, Ibaraki, Japan; cell no. RCB2202). HEK 293T cells were maintained in Dulbecco's modified Eagle's medium (Life Technologies, Carlsbad, CA, USA) supplemented with 10% (v/v) fetal bovine serum, 100 U/ml of penicillin G, and 100 μg/ml of streptomycin (Life Technologies). Cells were cultured at 37°C in a 5% CO_2 atmosphere.

Viral Vector Production and Titration

HEK 293T cells were plated in 4×150 mm dishes, and the following day the cells were transfected with 100 μg transfer plasmid, 20 μg envelope plasmid, 20 μg pCAG4-RTR2, and 20 μg pCAG-kGP1.1R, using the calcium phosphate method. The detailed procedure for virus production has been described previously (54). For comprehensive information on plasmids, please see Table S2. The titers of FuGB2 vectors were determined by the DNA titration method as previously described (56). Briefly, cultured HEK 293T cells were transduced, their genomic DNA was extracted, and the copy number of integrated lentiviral genomes was analyzed by performing TaqMan real-time PCR for the Woodchuck hepatitis virus post-transcriptional regulatory element (WPRE) sequence (56). Titers of the Env vectors were determined by the RNA titration method (57) using the Lenti-X qRT-PCR Titration Kit (Clontech Laboratories).

Fluorescence Microscopic Imaging and Flow-Cytometric Analysis of HEK 293T cells

HEK 293T cells were plated in 60 mm dishes (1×10^5 cells/dish), and the FuGB2 vector solution was added to the medium (multiplicity of infection [MOI] = 5) the same day. Three days later, the infected HEK 293T cells were collected and seeded in 6-well plates (1×10^5 cells/well). After cells were plated, one of the Env vector solutions was added (MOI=100). For fluorescence microscopy, 3 days after infection with the Env vector, infected HEK 293T cells were collected and passaged (1×10^5 cells/well) in 4-well plates (Becton Dickinson) coated with collagen I (Becton Dickinson, Mountain View, USA). After plating, HEK 293T cells were fixed with 4% (w/v) paraformaldehyde (PFA) in phosphate-buffered saline (PBS) at room temperature for 15 min. After washing with PBS, 4-well plates were coverslipped using Fluoroshield Mounting Medium (ImmunoBioScience, Mukilteo, WA, USA) and examined using a Zeiss LSM 780 confocal microscope (Carl Zeiss Microscopy, Weesp, Netherlands). For flow cytometry, 3 days after infection with the Env vector, HEK 293T cells were harvested and fixed with 2% (w/v) PFA in PBS at 4°C for 15 min. Cells were resuspended in 1.0 ml PBS, and then filtered through a 40 μm nylon membrane (Kyoshin Rikoh, Tokyo, Japan). Samples of 10,000 cells were analyzed, and the fraction of AcGFP1- or mCherry-positive cells was determined using an EPICS XL flow cytometer equipped with the EXPO 32 software (Beckman Coulter, Brea, CA, USA) and FlowJo software (Tree Star, Ashland, OR, USA) (25).

Surgical Procedures and Viral Injections into Rat Cortices and Thalamus
Ten-week-old male Wistar rats (Nihon SLC, Hamamatsu, Japan) were housed in groups (three or four animals per cage) and had free access to rat pellet chow and water. Each rat

was anesthetized with a mixture of ketamine and xylazine (90 mg/kg and 10 mg/kg, respectively) injected intraperitoneally. Rats were positioned in a stereotactic frame (SR-6R; Narishige, Tokyo, Japan), and body temperature was maintained at 37°C using a rectal probe and a heating pad (BWT-100A; BRC, Nagoya, Japan). An incision was made in the scalp, and a small craniotomy was made to target the injection area. The dura was punctured, and the virus was delivered via a 32-gauge needle attached to a 10-μl gas-tight Hamilton syringe (Hamilton Company, Reno, NV, USA). After the injection, the scalp was sutured.

Viral vectors were injected into the rats twice. First, one or all three receptor-expressing vectors were injected into the somatosensory cortices, and second, a mixture of EnvA/B/E vectors was injected into the thalamus. In the first injection, 1.5 μl of FuGB2 vector (titer: 4.0×10^{10} transduction units per mL [TU/mL]) was injected to a depth of 600 μm below the dura surface at the rate of 100 nl/min for 15 min. The injection sites were as follows: FuGB2-TVA950 vector, anterior +1.5 mm from bregma and lateral 3.9 mm from the midline; FuGB2-TVB^{S3} vector, anterior −0.5 mm and lateral 3.9 mm; FuGB2-DR-46TVB vector, anterior −2.5 mm and lateral 3.9 mm. The second injection was conducted 3 weeks after the first injection. Env vectors (4.0 μl; a mixture of Env vectors, each adjusted to 2.0×10^{10} TU/ml) were injected into the thalamus (anterior = −3.0 mm, lateral = 2.5 mm, and depth = 5.5 mm) for 40 min.

Immunohistochemistry

22

Histology was performed as previously described (25). Three weeks after Env vector injection, rats were transcardially perfused with saline and 4% (w/v) PFA in PBS. The brains were then post-fixed in 4% PFA in PBS for 6 h, processed in 20% (w/v) sucrose in PBS, and embedded in optimum cutting temperature (OCT) compound (Sakura, Tokyo, Japan). Brains were frozen with dry ice and cut into 25-μm thick sections using a cryostat (Leica CM 3050S, Wetzlar, Germany).

The immunohistochemistry was performed as described previously, with modifications[39]. Brain sections were incubated in a blocking solution of 5% normal goat serum (NGS, Vector Laboratories, Burlingame, USA) and 0.3% Triton X-100 in PBS for 30 min at room temperature, and subsequently incubated with primary antibodies (with 5% NGS and 0.3% Triton X-100 in PBS) for 3 days at 4°C. On the last day, brain sections were incubated with secondary antibodies for 1 h at room temperature. After thorough washing, the sections were incubated with antibody against NeuN or the appropriate epitope tag (for cell counting) for 2 days at 4°C. The sections were incubated with biotin-conjugated goat anti-mouse antibody (1:500; Vector, BA-9200) in blocking solution for 30 min, and then with Alexa Fluor 647 streptavidin (1:500; Molecular Probes, S-21374) for 1 h at room temperature. Sections were coverslipped using i-BRITE Plus (Neuromics, Bloomington, IN, USA) and stored at −20°C.

For BFP, EGFP, tdTomato, and NeuN staining, brain sections were visualized using the following primary antibodies: chicken anti-GFP (1:1000; Genetex, GTX13970), rabbit anti-tRFP (1:1000; Evrogen, AB233), mouse anti-DsRed (1:1000; Clontech, 632393), and mouse anti-NeuN (1:1000; Millipore, MAB377). For cell count sections, fluorescence

staining was also conducted using the same primary antibodies as described above, and each epitope tag was visualized using the following primary antibodies: mouse anti-HA (1:1000; Covance, MMS-101R), mouse anti–c-Myc (1:1000; MBL, M192-3S), or mouse anti–FLAG M2 (1:1000; Sigma-Aldrich, F1804). The secondary antibodies used were goat anti-chicken Alexa Fluor 488 (1:500; Molecular Probes, A11039), goat anti-rabbit Alexa Fluor 405 (1:500; Molecular Probes, A31556), and goat anti-mouse Alexa Fluor 546 (1:500; Molecular Probes, A11035).

Image Collection and Cell Counting

Images of triple-colored cells and sections were captured using a Zeiss LSM 780 confocal microscope and analyzed using the ZEN Lite 2012 software (Carl Zeiss Microscopy, Weesp, Netherlands). For cell counting, sections were imaged on a Keyence BZ-9000 Biorevo all-in-one fluorescence microscope using the BZ-II analysis application (KEYENCE, Osaka, Japan). The same sections were also imaged on a Leica TCS SPE confocal microscope using LAS AF Lite software (Leica). Quantitative *in vivo* data were obtained from sections stained to detect epitope tags. Five non-adjacent sections (every third section) were chosen in each rat. All fluorescence-positive and epitope tag–positive neurons were manually counted from all fields of the sections. In order to determine the specificity of receptor–envelope pairs *in vivo*, the percentage of fluorescence-positive neurons that were also positive for the epitope tag (i.e., double-positive cells) was calculated.

Statistical Analysis

For statistical analysis, the data were evaluated for significance by performing one-way ANOVA followed by Scheffe's F-test using Excel (Microsoft, Seattle, WA, USA). Percentage values were arcsine-transformed prior to statistical analysis. P-values less than 0.01 were considered to represent statistically significant differences. Unless otherwise indicated, data are presented as means and standard error of the mean (SEM).

Acknowledgements

References

1. Felleman DJ & Van Essen DC (1991) Distributed hierarchical processing in the primate cerebral cortex. *Cereb. Cortex* 1(1):1-47.

2. Miyashita Y (2004) Cognitive memory: cellular and network machineries and their top-down control. *Science* 306(5695):435-440.

3. Pennartz CM*, et al.* (2009) Corticostriatal Interactions during Learning, Memory Processing, and Decision Making. *The Journal of neuroscience : the official journal of the Society for Neuroscience* 29(41):12831-12838.

4. Wang SH & Morris RG (2010) Hippocampal-neocortical interactions in memory formation, consolidation, and reconsolidation. *Annual review of psychology* 61:49-79, C41-44.

5. Dum RP & Strick PL (2013) Transneuronal tracing with neurotropic viruses reveals network macroarchitecture. *Curr Opin Neurobiol* 23(2):245-249.

6. Sternberg N & Hamilton D (1981) Bacteriophage P1 site-specific recombination. I. Recombination between loxP sites. *J Mol Biol* 150(4):467-486.

7. Gossen M & Bujard H (1992) Tight control of gene expression in mammalian cells by tetracycline-responsive promoters. *Proceedings of the National Academy of Sciences of the United States of America* 89(12):5547-5551.

8. Wickersham IR*, et al.* (2007) Monosynaptic restriction of transsynaptic tracing from single, genetically targeted neurons. *Neuron* 53(5):639-647.

9. Luo L, Callaway EM, & Svoboda K (2008) Genetic dissection of neural circuits. *Neuron* 57(5):634-660.

10. Guillery RW & Sherman SM (2002) Thalamic relay functions and their role in corticocortical communication: generalizations from the visual system. Neuron 33(2):163-175.

11. Grove J & Marsh M (2011) The cell biology of receptor-mediated virus entry. *J Cell Biol* 195(7):1071-1082.

12. Barnard R, Elleder D, & Young J (2006) Avian sarcoma and leukosis virus-receptor interactions: from classical genetics to novel insights into virus-cell membrane fusion. *Virology* 344(1):25-29.

13. Elleder D, Melder D, Trejbalova K, Svoboda J, & Federspiel M (2004) Two different molecular defects in the Tva receptor gene explain the resistance of two tvar lines of chickens to infection by subgroup A avian sarcoma and leukosis viruses. *J. Virol.* 78(24):13489-13500.

14. Brojatsch J, Naughton J, Rolls M, Zingler K, & Young J (1996) CAR1, a TNFR-related protein, is a cellular receptor for cytopathic avian leukosis-sarcoma viruses and mediates apoptosis. *Cell* 87(5):845-855.

15. Elleder D*, et al.* (2005) The receptor for the subgroup C avian sarcoma and leukosis viruses, Tvc, is related to mammalian butyrophilins, members of the immunoglobulin superfamily. *J. Virol.* 79(16):10408-10419.

16. Adkins H*, et al.* (1997) Identification of a cellular receptor for subgroup E avian leukosis virus. *Proceedings of the National Academy of Sciences of the United States of America* 94(21):11617-11622.

17.   Chai N & Bates P (2006) Na+/H+ exchanger type 1 is a receptor for pathogenic subgroup J avian leukosis virus. *Proceedings of the National Academy of Sciences of the United States of America* 103(14):5531-5536.

18.   Adkins HB, Brojatsch J, & Young JA (2000) Identification and characterization of a shared TNFR-related receptor for subgroup B, D, and E avian leukosis viruses reveal cysteine residues required specifically for subgroup E viral entry. *J Virol* 74(8):3572-3578.

19.   Duff RG & Vogt PK (1969) Characteristics of two new avian tumor virus subgroups. *Virology* 39(1):18-30.

20.   Boettiger D, Love DN, & Weiss RA (1975) Virus envelope markers in mammalian tropism of avian RNA tumor viruses. *J Virol* 15(1):108-114.

21.   Bova CA, Olsen JC, & Swanstrom R (1988) The avian retrovirus env gene family: molecular analysis of host range and antigenic variants. *J Virol* 62(1):75-83.

22.   Marshel JH, Mori T, Nielsen KJ, & Callaway EM (2010) Targeting single neuronal networks for gene expression and cell labeling in vivo. *Neuron* 67(4):562-574.

23.   Miyamichi K*, et al.* (2013) Dissecting local circuits: parvalbumin interneurons underlie broad feedback control of olfactory bulb output. *Neuron* 80(5):1232-1245.

24.   Bachmair A, Finley D, & Varshavsky A (1986) In vivo half-life of a protein is a function of its amino-terminal residue. *Science* 234(4773):179-186.

25.   Yaguchi M*, et al.* (2013) Characterization of the properties of seven promoters in the motor cortex of rats and monkeys after lentiviral vector-mediated gene transfer. *Hum Gene Ther Methods* 24(6):333-344.

26. Wickersham IR, Finke S, Conzelmann KK, & Callaway EM (2007) Retrograde neuronal tracing with a deletion-mutant rabies virus. *Nat Methods* 4(1):47-49.

27. Klucking S & Young JA (2004) Amino acid residues Tyr-67, Asn-72, and Asp-73 of the TVB receptor are important for subgroup E avian sarcoma and leukosis virus interaction. *Virology* 318(1):371-380.

28. Parks DR, Roederer M, & Moore WA (2006) A new "Logicle" display method avoids deceptive effects of logarithmic scaling for low signals and compensated data. *Cytometry. Part A : the journal of the International Society for Analytical Cytology* 69(6):541-551.

29. Agmon A & Connors BW (1991) Thalamocortical responses of mouse somatosensory (barrel) cortex in vitro. *Neuroscience* 41(2-3):365-379.

30. Staiger JF, Kotter R, Zilles K, & Luhmann HJ (1999) Connectivity in the somatosensory cortex of the adolescent rat: an in vitro biocytin study. *Anat Embryol (Berl)* 199(4):357-365.

31. Cruikshank SJ, Rose HJ, & Metherate R (2002) Auditory thalamocortical synaptic transmission in vitro. *J Neurophysiol* 87(1):361-384.

32. MacLean JN, Fenstermaker V, Watson BO, & Yuste R (2006) A visual thalamocortical slice. *Nat Methods* 3(2):129-134.

33. Makoto M, Yohei O, Tadashi T, Masae Y, Shigeki K, Kazuto K, & Yasushi M (2015) Avian sarcoma leukosis virus receptor-envelope system for simultaneous dissection of multiple neural circuit in mammalian brain. *Proceedings of the National Academy of Sciences of the United States of America* 112(22):E2947-561.

34. Hirano M, Kato S, Kobayashi K, Okada T, & Yaginuma H (2013) Highly efficient retrograde gene transfer into motor neurons by a lentiviral vector pseudotyped with fusion glycoprotein. *PloS one* 8(9):e75896.

35. Lu X, Miyachi S, & Takada M (2012) Anatomical evidence for the involvement of medial cerebellar output from the interpositus nuclei in cognitive functions. *Proceedings of the National Academy of Sciences of the United States of America* 109(46):18980-18984.

36. Hirata Y*, et al.* (2013) Dorsal area 46 is a major target of disynaptic projections from the medial temporal lobe. *Cereb Cortex* 23(12):2965-2975.

37. Miyachi S*, et al.* (2013) Multisynaptic projections from the ventrolateral prefrontal cortex to hand and mouth representations of the monkey primary motor cortex. *Neuroscience research* 76(3):141-149.

38. Kelly RM & Strick PL (2000) Rabies as a transneuronal tracer of circuits in the central nervous system. *J Neurosci Methods* 103(1):63-71.

39. Nguyen TD*, et al.* (2012) Targeted single-neuron infection with rabies virus for transneuronal multisynaptic tracing. *J Neurosci Methods* 209(2):367-370.

40. Mothes W, Boerger AL, Narayan S, Cunningham JM, & Young JA (2000) Retroviral entry mediated by receptor priming and low pH triggering of an envelope glycoprotein. *Cell* 103(4):679-689.

41. Lewis BC, Chinnasamy N, Morgan RA, & Varmus HE (2001) Development of an avian leukosis-sarcoma virus subgroup A pseudotyped lentiviral vector. *J. Virol.* 75(19):9339-9344.

42. Babel AR, Bruce J, & Young JA (2007) The hr1 and fusion peptide regions of the subgroup B avian sarcoma and leukosis virus envelope glycoprotein influence low pH-dependent membrane fusion. *PloS one* 2(1):e171.

43. Barnard RJ, Elleder D, & Young JA (2006) Avian sarcoma and leukosis virus-receptor interactions: from classical genetics to novel insights into virus-cell membrane fusion. *Virology* 344(1):25-29.

44. Boyden ES, Zhang F, Bamberg E, Nagel G, & Deisseroth K (2005) Millisecond-timescale, genetically targeted optical control of neural activity. *Nat Neurosci* 8(9):1263-1268.

45. Han X*, et al.* (2009) Millisecond-timescale optical control of neural dynamics in the nonhuman primate brain. *Neuron* 62(2):191-198.

46. Yamamoto M*, et al.* (2003) Reversible suppression of glutamatergic neurotransmission of cerebellar granule cells in vivo by genetically manipulated expression of tetanus neurotoxin light chain. *The Journal of neuroscience : the official journal of the Society for Neuroscience* 23(17):6759-6767.

47. Nakashiba T, Young JZ, McHugh TJ, Buhl DL, & Tonegawa S (2008) Transgenic inhibition of synaptic transmission reveals role of CA3 output in hippocampal learning. *Science* 319(5867):1260-1264.

48. Nakashiba T, Buhl DL, McHugh TJ, & Tonegawa S (2009) Hippocampal CA3 output is crucial for ripple-associated reactivation and consolidation of memory. *Neuron* 62(6):781-787.

49.   Tan EM*, et al.* (2006) Selective and quickly reversible inactivation of mammalian neurons in vivo using the Drosophila allatostatin receptor. *Neuron* 51(2):157-170.

50.   Inoue K*, et al.* (2012) Immunotoxin-mediated tract targeting in the primate brain: selective elimination of the cortico-subthalamic "hyperdirect" pathway. *PloS one* 7(6):e39149.

51.   Takada M*, et al.* (2013) Elucidating information processing in primate basal ganglia circuitry: a novel technique for pathway-selective ablation mediated by immunotoxin. *Frontiers in neural circuits* 7:140.

52.   Zhang F*, et al.* (2008) Red-shifted optogenetic excitation: a tool for fast neural control derived from Volvox carteri. *Nat Neurosci* 11(6):631-633.

53.   Berndt A, Yizhar O, Gunaydin LA, Hegemann P, & Deisseroth K (2009) Bi-stable neural state switches. *Nat Neurosci* 12(2):229-234.

54.   Ohashi Y*, et al.* (2011) A bicistronic lentiviral vector-based method for differential transsynaptic tracing of neural circuits. *Mol Cell Neurosci* 46(1):136-147.

55.   Brojatsch J, Naughton J, Adkins HB, & Young JA (2000) TVB receptors for cytopathic and noncytopathic subgroups of avian leukosis viruses are functional death receptors. *J. Virol.* 74(24):11490-11494.

56.   Tsubota T, Ohashi Y, Tamura K, Sato A, & Miyashita Y (2011) Optogenetic manipulation of cerebellar Purkinje cell activity in vivo. *PloS one* 6(8):e22400.
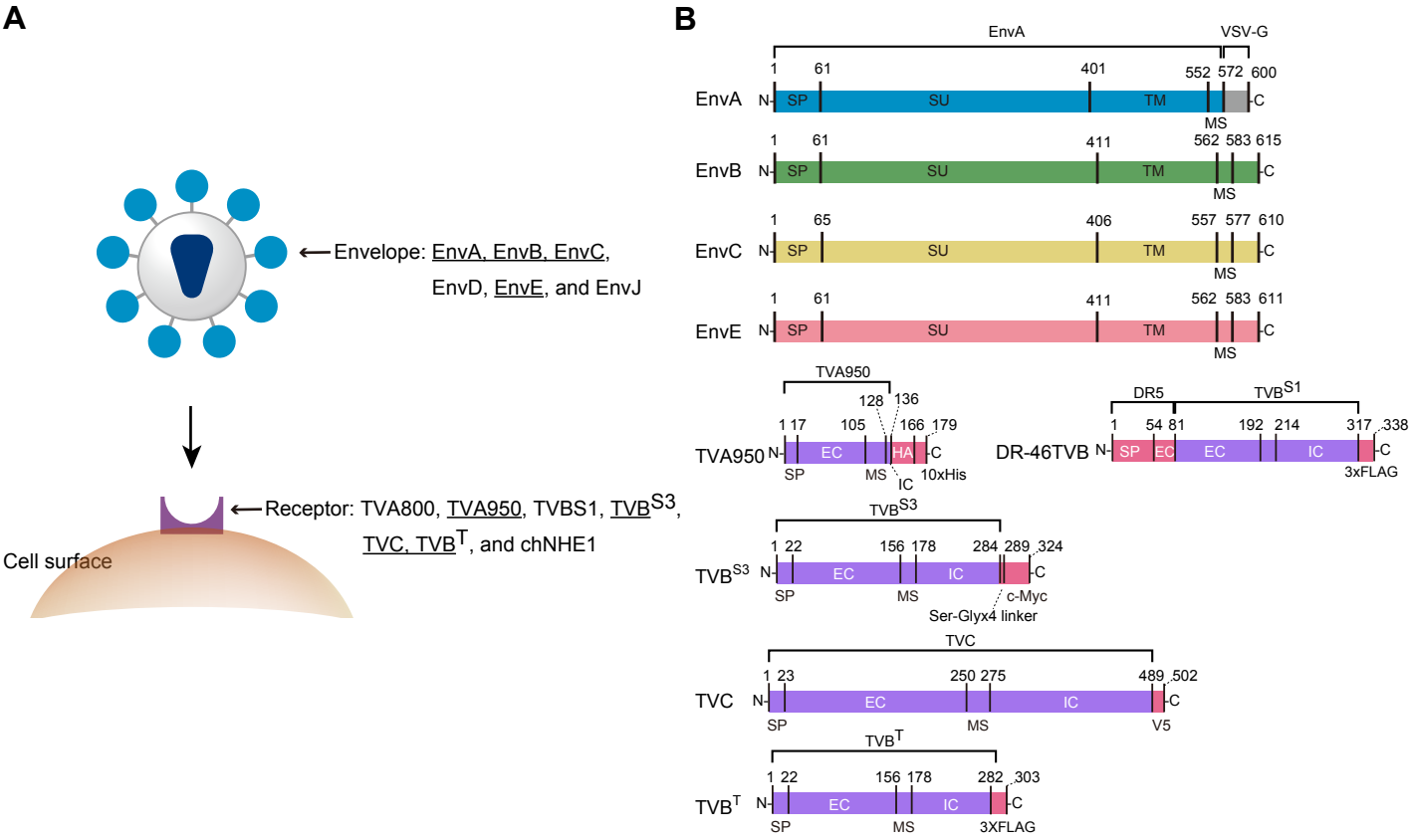
57.   Kato S, *et al.* (2011) A lentiviral strategy for highly efficient retrograde gene transfer by pseudotyping with fusion envelope glycoprotein. *Hum Gene Ther* 22(2):197-206.

Table 1. The orthogonality of the receptor–envelope combinations *in vivo*. Number of
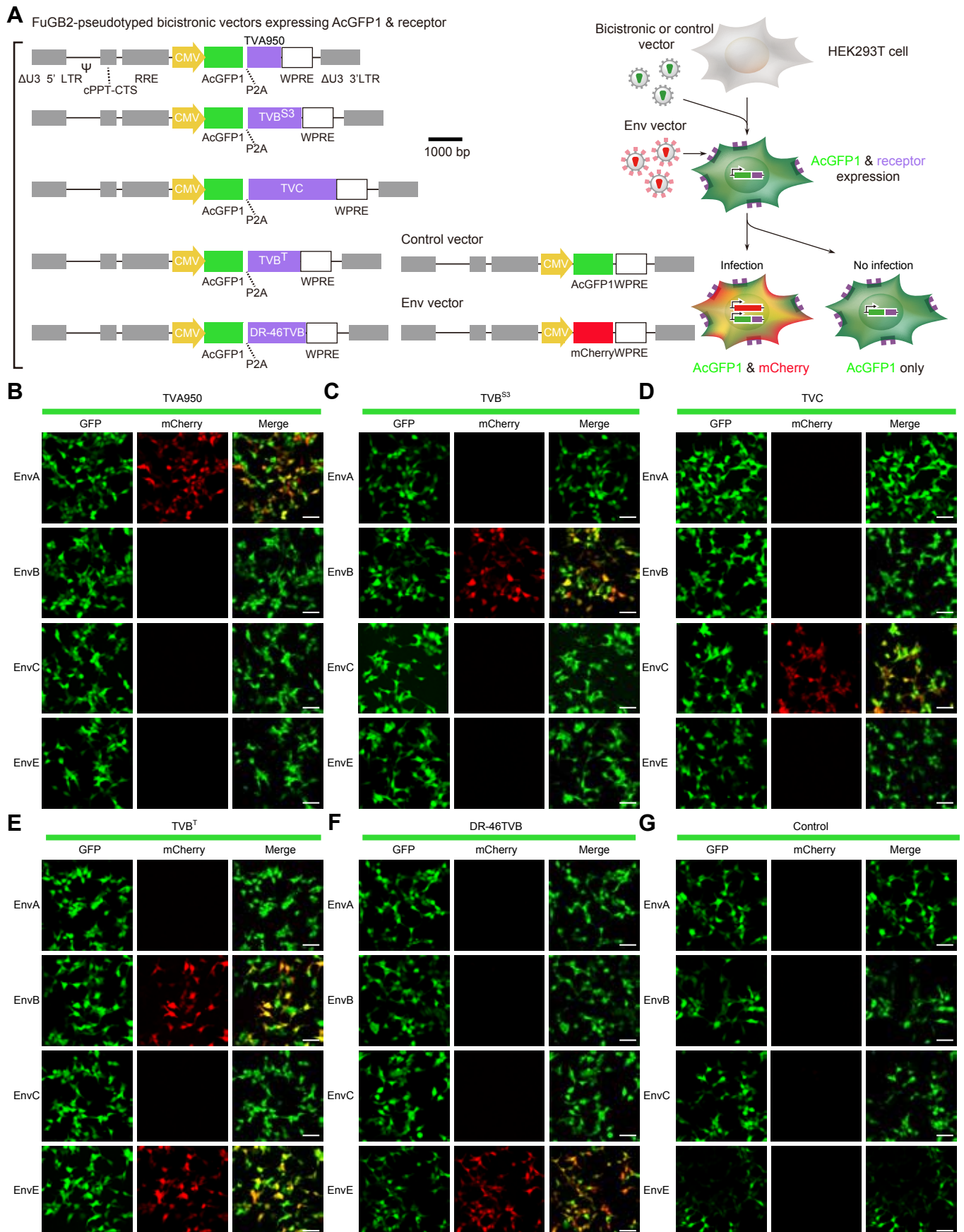BFP-, EGFP-, tdTomato-, and receptor-positive neurons in rats

Env vector	Receptor	Rat number	Number of sections	Number of BFP+ neurons		Number of EGFP+ neurons		Number of tdTomato+ neurons	
				TVA950+	TVA950-	TVA950+	TVA950-	TVA950+	TVA950-
EnvA-BFP & EnvB-EGFP & EnvE-tdTomato	TVA950	A1	5	572	8	0	0	0	0
		A2	5	974	8	0	0	0	0
		A3	5	1942	17	0	0	0	0
				TVBS3+	TVBS3-	TVBS3+	TVBS3-	TVBS3+	TVBS3-
	TVB^{S3}	B1	5	0	0	1200	12	0	0
		B2	5	0	0	384	13	0	0
		B3	5	0	0	954	10	0	0
				DR-46TVB+	DR-46TVB-	DR-46TVB+	DR-46TVB-	DR-46TVB+	DR-46TVB-
	DR-46TVB	D1	5	0	0	0	0	400	2
		D2	5	0	0	0	0	501	1
		D3	5	0	0	0	0	222	0

Note: Table 1, related to Figures 4, 5, and 6: Distribution of fluorescent-positive neurons
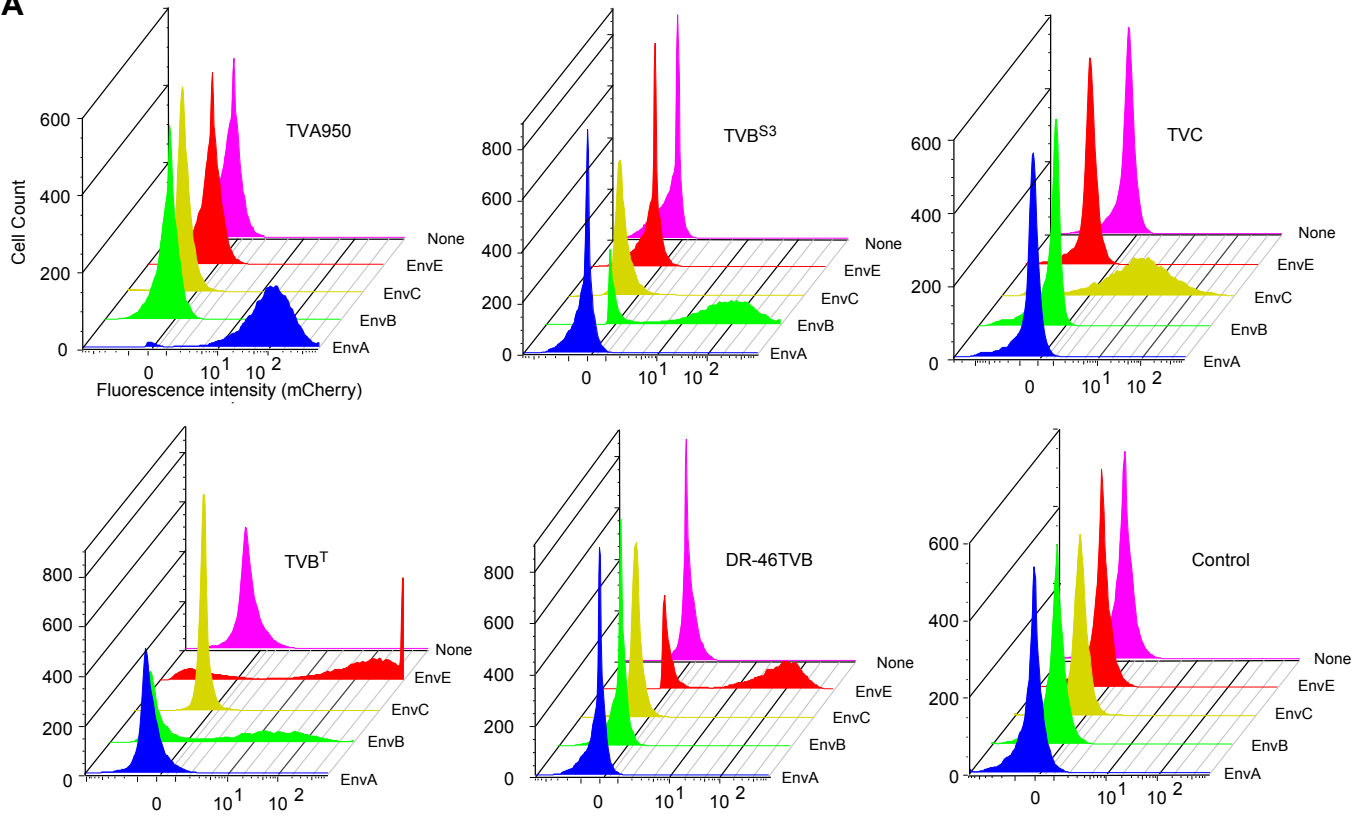in individual animals.
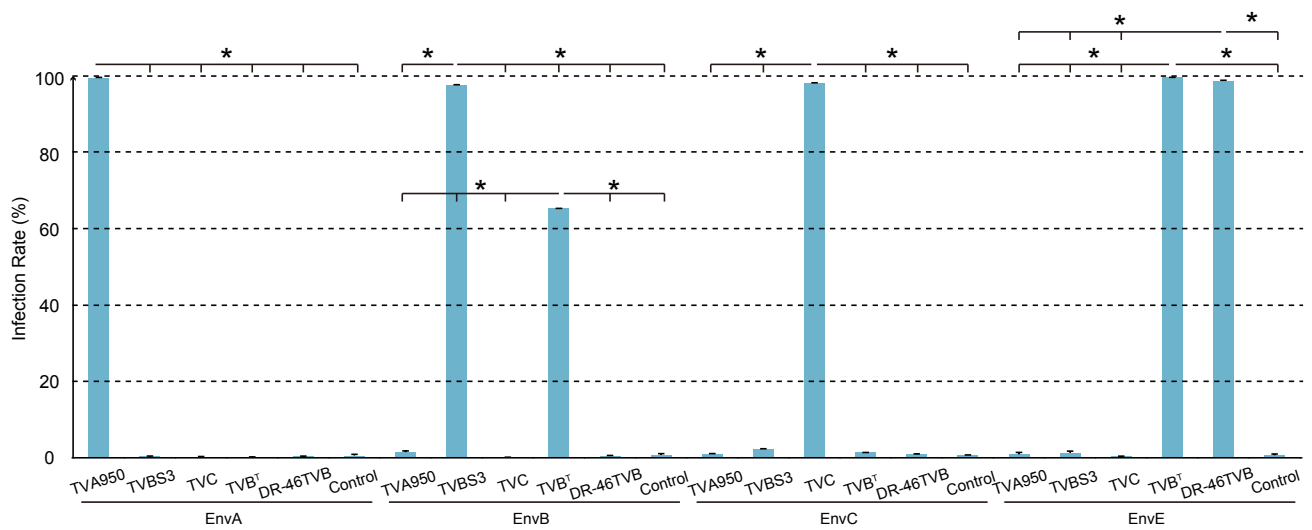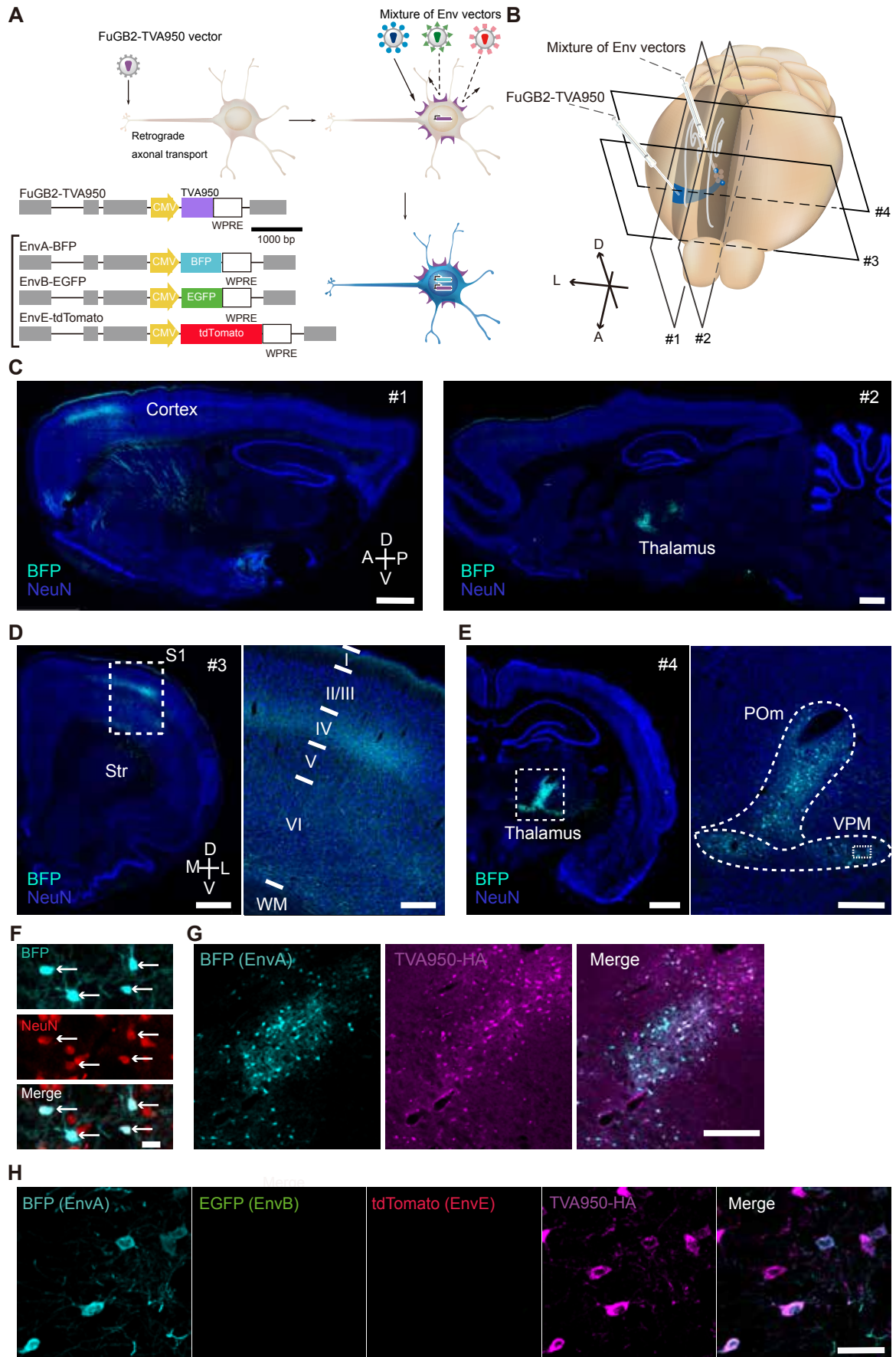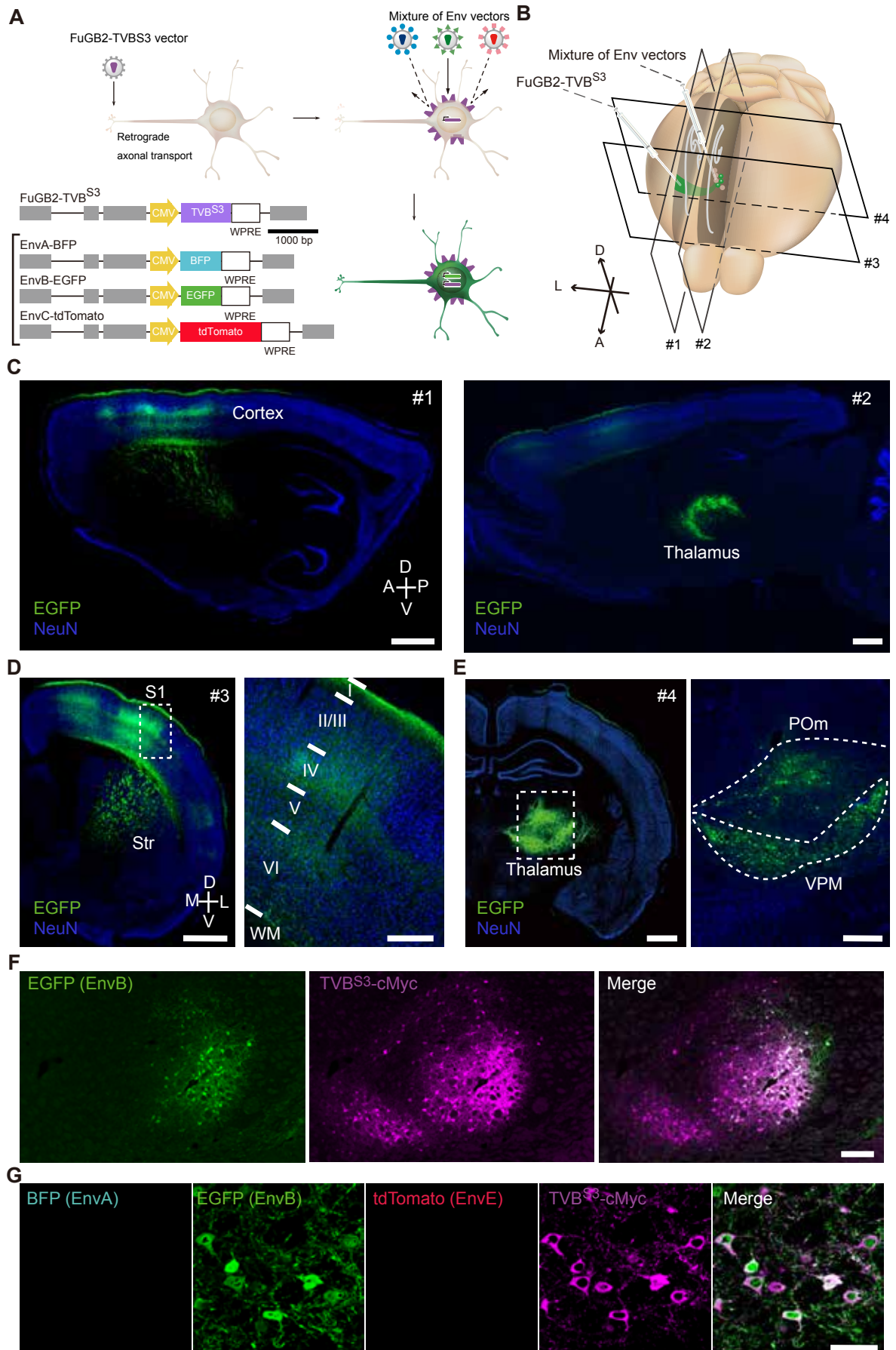
Figure 1

Figure 2

A FuGB2-pseudotyped bicistronic vectors expressing AcGFP1 & receptor

Figure 3

Figure 4

Figure 5

Figure 6

Figure 7

A

FuGB2-TVA950

FuGB2-TVBS3

FuGB2-DR-46TVB

1000 bp

EnvA-BFP

EnvB-EGFP

EnvE-tdTomato

Mixture of Env vectors

EnvA vector   EnvB vector   EnvE vector

TVA950 expression   TVBS3 expression   DR-46TVB expression

Mixture of Gate-expressing cells

B

BFP   EGFP   tdTomato   Merge
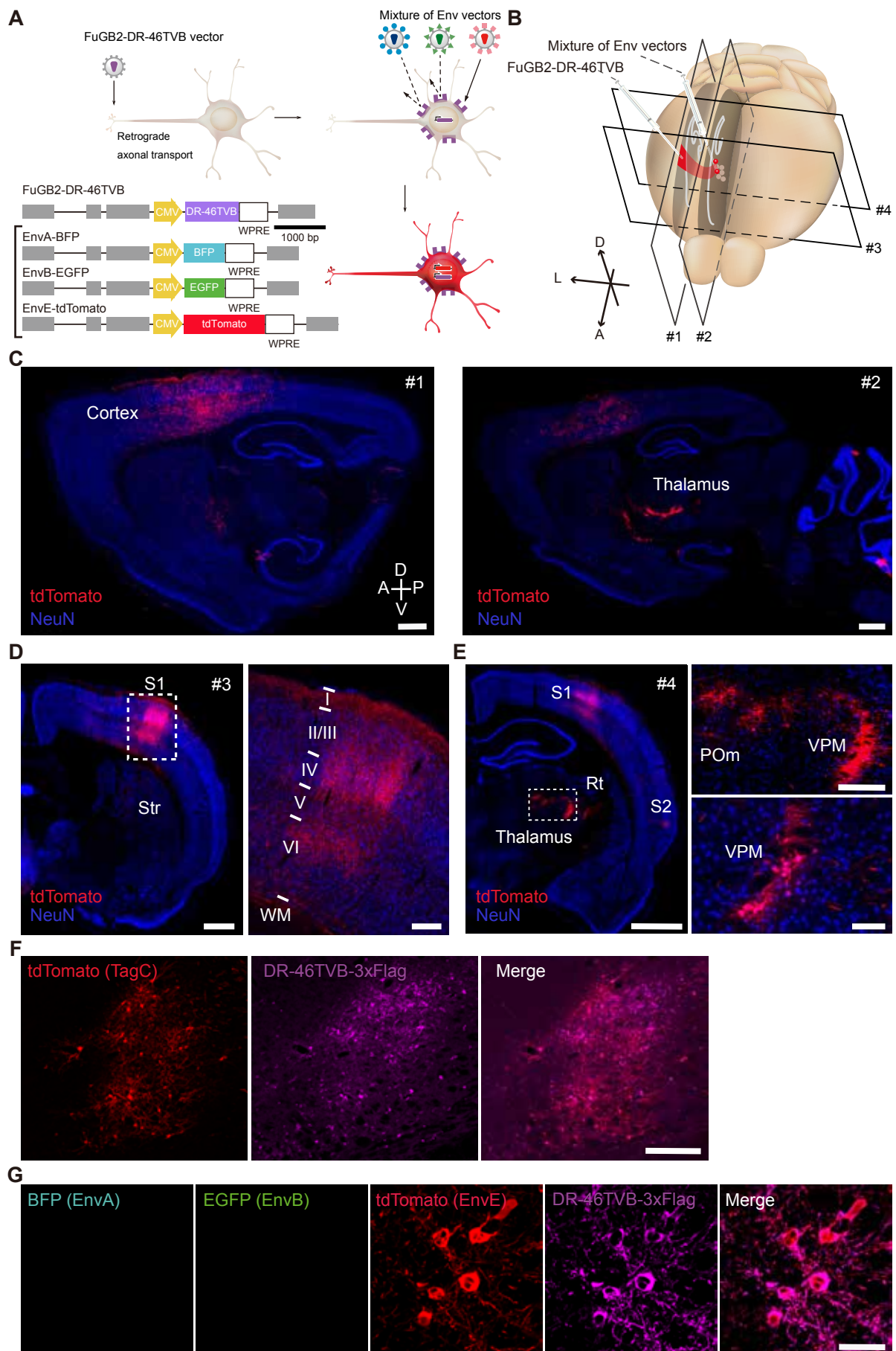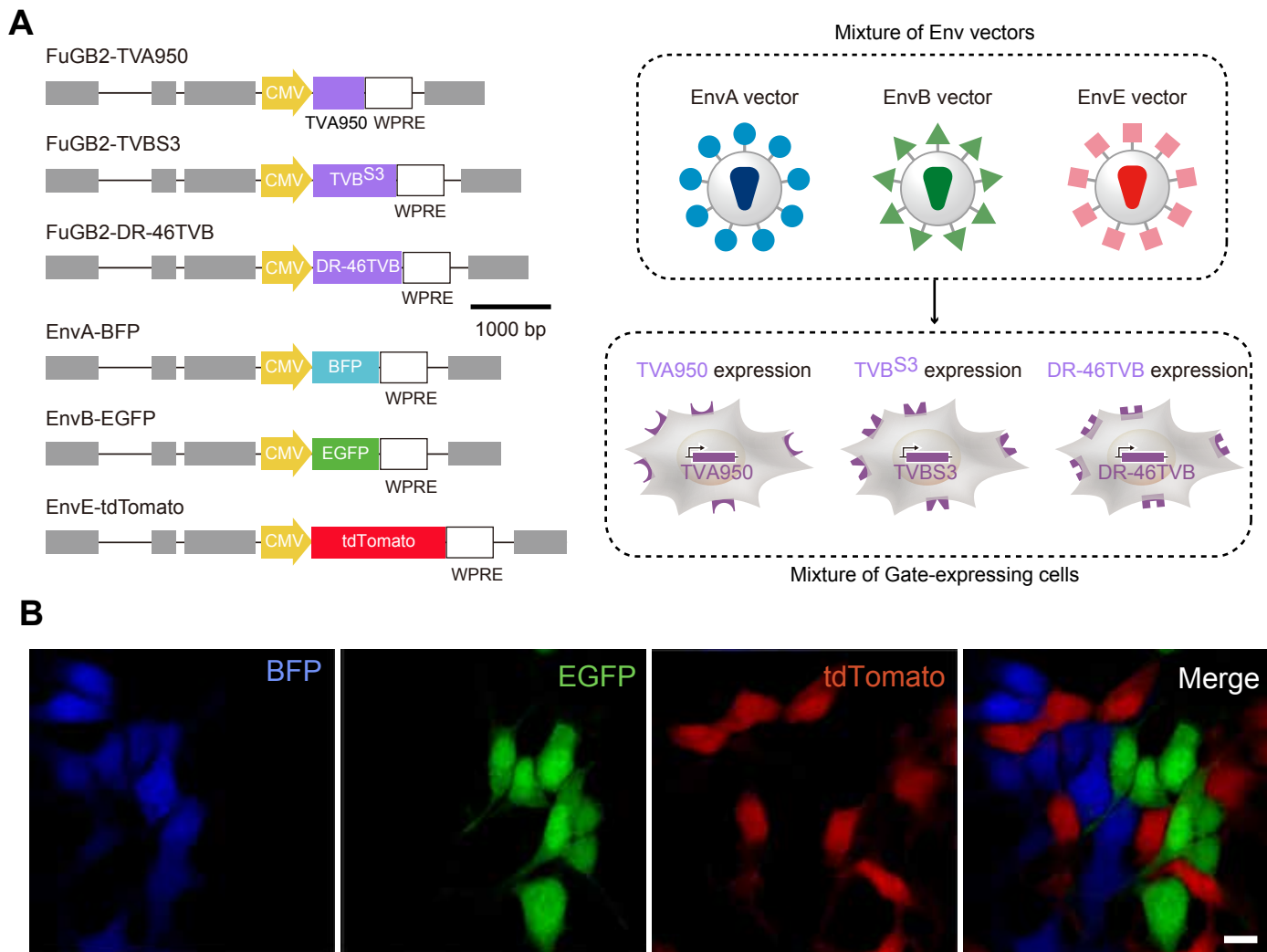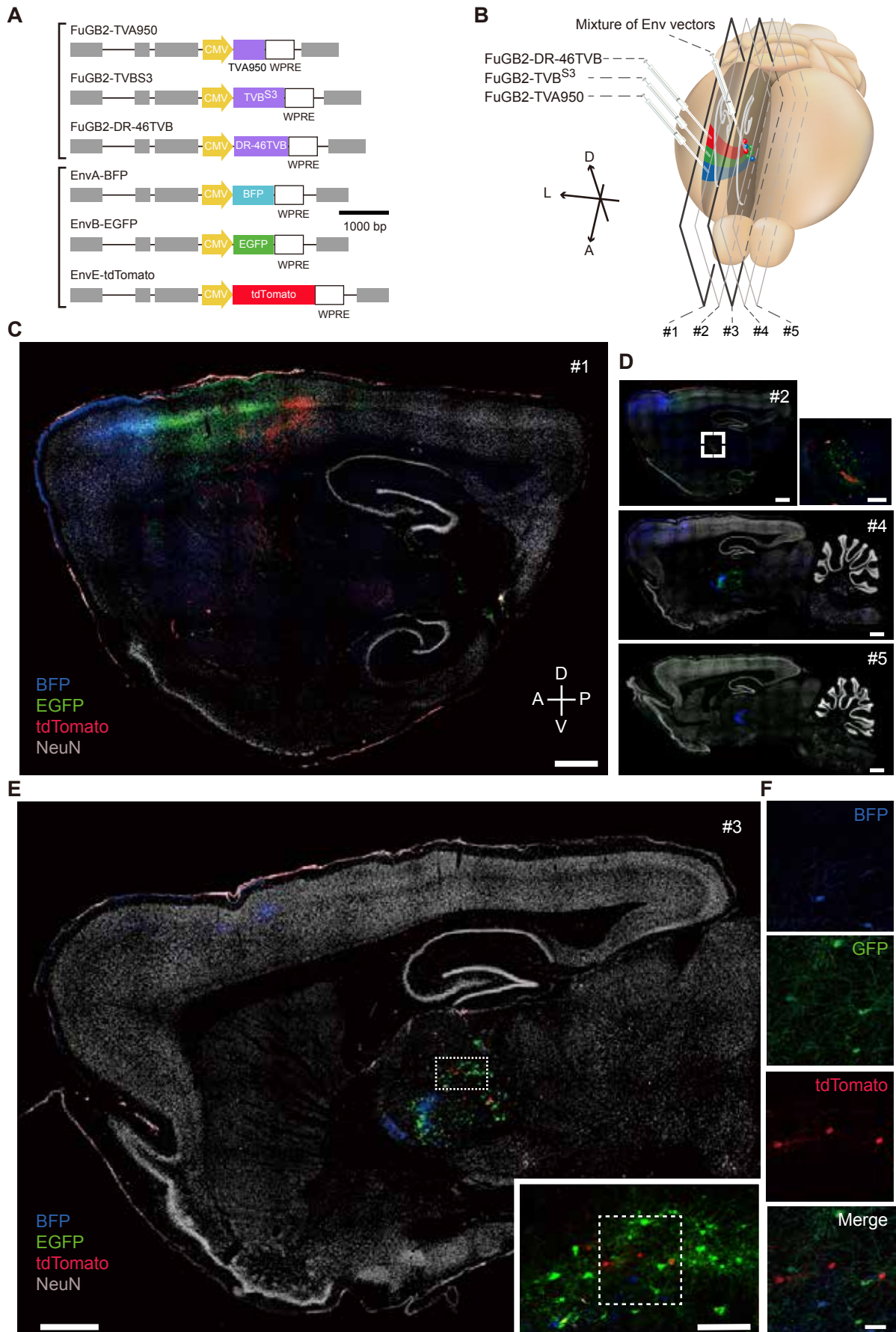
Figure 8

Figure Legends

Figure 1. Selection and construction of ASLV-pseudotyped lentiviral vectors and avian-derived receptors. (**A**) Schematic illustration of receptors expressed on the cell surface and their specificity for avian sarcoma leukosis virus (ASLV) envelope–pseudotyped lentiviral entry. The ASLV receptors and envelopes used in the following experiments were underlined. (**B**) Schematic illustration of the altered ASLV receptors and envelopes constructs used in this study. Numbers indicate the position of amino-acid residues in mature proteins; signal peptide residues have positive numbers. SU, surface envelope subunit; TM, transmembrane envelope subunit; VSV-G, vesicular stomatitis virus G protein; SP, signal peptide; EC, extracellular domain; MS, transmembrane spanning domain; IC, intracellular domain; HA, epitope tag from influenza virus HA protein; His, histidine residue tag; Ser-Glyx4 linker, 5-amino-acid peptide normally used as the linker; DR5, DEATH RECEPTOR 5. Adapted from Matsuyama et al. (2015).

Figure 2. Characterization of ASLV receptor-envelope pairs *in vitro*. (**A**) Schematic representation of the lentiviral vector constructs used *in vitro* and the experimental outline of serial infections of bicistronic vectors and Env vectors in HEK 293T cells. cPPT, central polypurine tract; CTS, central termination sequence; LTR, long terminal repeat; RRE, Rev responsive element; Ψ, packaging signal; CMV, cytomegalovirus promoter; P2A, picornaviral 2A peptide; WPRE, Woodchuck hepatitis virus post-transcriptional regulatory element. (**B**–**G**) Fluorescence images of HEK 293T cells expressing TVA950 (B), TVB[S3]

(C), TVC (D), TVB^T (E), and DR-46TVB (F) after transfection with one of the Env vectors. Receptor proteins were co-expressed with AcGFP1. A vector expressing only *Aequorea coerulescens* green fluorescent protein (AcGFP1) was used as a negative control (G). Scale bars: 50 μm in (B–G). Adapted from Matsuyama et al. (2015).

Figure 3. Quantitative comparison of *in vitro* infection rates of all ASLV receptor–envelope pairs.

(**A**) Representative histograms of mCherry fluorescence intensity for every possible receptor–envelope pair expressed in HEK 293T cells. Receptor-expressing cells infected by EnvA-, EnvB-, EnvC-, or EnvE-pseudotyped vectors (blue, green, yellow, and red histograms) are compared to receptor-expressing cells infected with no Env vectors (purple histograms). In the control condition, HEK 293T cells were infected with AcGFP1-expressing vector instead of the bicistronic vector. The vertical axis represents the total number of counted cells, and the horizontal axis represents Logicle scaling (27). (**B**) Histograms showing the infection rates of Env vectors into HEK 293T cells positive for each receptor. Cells expressing AcGFP1 were considered receptor-positive. Thus, the infection rate is estimated by calculating the ratio of mCherry- and AcGFP1-positive cells to all AcGFP1-positive cells in flow-cytometry analysis. Three independent experiments were conducted, and the data were analyzed using one-way ANOVA followed by Scheffe's F-test (*$P < 0.001$). The average mean values of three experiments are shown, with the standard deviation of the data indicated by error bars. Adapted from Matsuyama et al. (2015).

Figure 4. Orthogonality of the TVA950–EnvA pair *in vivo***, demonstrated in rat thalamocortical neurons.** (**A**) Schematic representation of retrograde targeting of TVA950 expression through projection terminals and the selective entry of EnvA vectors from TVA950-expressing neuronal cell bodies. For clarity, EnvA/EnvB/EnvE are depicted as different shapes. (**B**) Stereotaxic coordinates of two-step viral injection. First, mutant rabies virus glycoprotein (FuGB2)-pseudotyped TVA950 vectors were injected into primary somatosensory cortex (S1). Three weeks after the first injection, a mixture of Env vectors was injected into the thalamus. (**C**) Overview of the rat brain sagittal sections counterstained with NeuN antibody. Merged images of NeuN (blue) and BFP (cyan) are shown. BFP-positive cells were restricted to the thalamus (C, right) and BFP-positive axons innervated S1 (C, left). Scale bars: 1000 μm. (**D**) A coronal section near the first injection site. The merged images show the distribution of BFP-positive axons. The boxed area (D, left) is magnified (D, right) to show the distribution of BFP-positive axons in the layers of S1. Scale bars: 1000 μm in D (left) and 250 μm in D (right). (**E**) A coronal section near the second injection site. The boxed area in the left panel is magnified (E, upper right) to show BFP-positive neurons in the ventral posteromedial (VPM) and posteromedian (POm) thalamic nuclei. Scale bars: 1000 μm in e (left), 250 μm in E (right). (**F**) The boxed area in Fig. 4E is further magnified to show double labeling of BFP (cyan)- and NeuN (red)-positive cells. Arrows indicate BFP-expressing cells. Scale bars: 25 μm. (**G**) A representative coronal section stained with anti-HA antibody. The merged image of BFP

(cyan) and TVA950-HA (purple) shows that BFP-positive neurons were a subpopulation of TVA950 (HA)-positive neurons. Scale bars: 250 μm. (**H**) Confocal images of a section stained with anti-HA antibody. BFP expression was observed in a subset of TVA950-HA–positive neurons, whereas expression of enhanced green fluorescent protein (EGFP) or tdTomato expression was not observed. Scale bars: 50 μm. Str, striatum; WM, white matter.Adapted from Matsuyama et al. (2015).

Figure 5. Orthogonality of the TVB^{S3}–EnvB pair *in vivo*, demonstrated in rat thalamocortical neurons. (**A**) Schematic representation of retrograde targeting of the TVB^{S3} expression through projection terminals and selective entry of EnvB vectors from TVB^{S3}-expressing neuronal cell bodies. (**B**) Stereotaxic coordinates of two-step viral injection. First, FuGB2-pseudotyped TVB^{S3} vectors were injected into primary somatosensory cortex (S1). Three weeks after the first injection, a mixture of Env vectors was injected into the thalamus. (**C**) Overview of the rat brain sagittal sections counterstained with NeuN antibody. The merged images of NeuN (blue) and EGFP (green) are shown. EGFP-positive cells were restricted to the thalamus (C, right), whereas EGFP-positive axons innervated S1 (C, left). Scale bars: 1000 μm. (**D**) Coronal section near the first injection site. Merged images show the distribution of EGFP-positive axons. The boxed area (D, left) is magnified (D, right) to show the distribution of EGFP-positive axons in the layers of S1. Scale bars: 1000 μm in D (left) and 250 μm in D (right). (**E**) Coronal section near the second injection site. The boxed area in the left panel is magnified (E, upper right) to show EGFP-positive neurons in the ventral posteromedial (VPM) and

posteromedian (POm) thalamic nuclei. The boxed area in the upper right panel is further magnified (E, lower right) to show double labeling of EGFP- and NeuN-positive cells. Scale bars: 1000 μm in E (left), 250 μm in E (upper right), and 50 μm in E (lower right). (**F**) Representative coronal section stained with anti-c-Myc antibody. The merged image of EGFP and TVB[S3]-c-Myc (purple) shows that EGFP-positive neurons were a subpopulation of the TVB[S3] (c-Myc)-positive neurons. Scale bars: 500 μm. (**G**) Confocal images of a section stained with anti-c-Myc antibody. EGFP expression was observed in a subset of TVB[S3]-c-Myc-positive neurons, whereas BFP or tdTomato expression was not observed. Scale bars: 50 μm. Adapted from Matsuyama et al. (2015).

Figure 6. Orthogonality of the DR-46TVB–EnvE pair *in vivo*, demonstrated in rat thalamocortical neurons. (**A**) Schematic representation of retrograde targeting of DR-46TVB expression through projection terminals and selective entry of EnvE vectors from DR-46TVB–expressing neuronal cell bodies. (**B**) Stereotaxic coordinates of two-step viral injection. First, FuGB2-pseudotyped DR-46TVB vectors were injected into the primary somatosensory cortex (S1). Three weeks after the first injection, a mixture of Env vectors was injected into the thalamus. (**C**) Overview of rat brain sagittal sections counterstained with NeuN antibody. Merged images of NeuN (blue) and tdTomato (red) are shown. tdTomato-positive cells were restricted to the thalamus (C, right), and tdTomato-positive axons innervated S1 (C, left). Scale bars: 1000 μm in C (left) and 250 μm in C (right). (**D**) Coronal section near the first injection site shows the distribution of tdTomato-positive

axons. The boxed area (D, left) is magnified (D, right) to show tdTomato-positive axons innervate layers I, IV, and VI in the S1. Scale bars: 1000 μm in D (left) and 250 μm in D (right). (**E**) Coronal section near the second injection site shows the distribution of tdTomato-positive neurons in detail. The boxed area (E, left) is magnified (E, right) to show tdTomato-positive neurons in the ventral posteromedial (VPM) and posteromedian (POm) thalamic nuclei. Scale bars: 1000 μm in E (left), 250 μm in E (upper right) and 100 μm in E (lower right). (**F**) Representative coronal section stained with anti-FLAG antibody. The merged image of tdTomato (red) and DR-46TVB-3×FLAG (purple) shows that tdTomato-positive neurons were a subpopulation of DR-46TVB (3×FLAG)-positive neurons. Scale bars: 500 μm. (**G**) Confocal images of a section stained with anti-FLAG antibody. tdTomato expression was observed in a subset of DR-46TVB-3×FLAG–positive neurons, whereas BFP (cyan) or EGFP (green) expression was not observed. Scale bars: 50 μm. S2, secondary somatosensory cortex; Rt, reticular thalamic nucleus. Adapted from Matsuyama et al. (2015).

Figure 7. Simultaneous gene transfer into multiple target cells *in vitro*. (**A**) Schematic representation of the lentiviral vector constructs used in this test, and experimental outline of the infection of HEK 293T cells with receptor-expressing vector and a mixture of Env vectors. (**B**) Fluorescence images of an intermingled population of HEK 293T cells expressing one of the three receptors transduced with a mixture of Env vectors expressing blue fluorescent protein (BFP), enhanced green fluorescent protein (EGFP), and tdTomato. Scale bar: 10 μm. Adapted from Matsuyama et al. (2015).

Figure 8. Fluorescent dissociation of three thalamic neuronal populations, each projecting to different cortical regions, visualized simultaneously with orthogonal receptor–envelope pairs. (**A**) Schematic representation of the lentiviral vector constructs used in this test. (**B**) Stereotaxic coordinates of two-step viral injection. First, each retrograde TVA950/TVB^{S3}/DR-46TVB-expressing vector was injected into the different primary somatosensory cortices. Three weeks after the first injection, a mixture of Env vectors was injected into the thalamus. The locations of the serial sections shown in (C–E) are depicted as #1, #2, #3, #4, and #5. (**C**–**E**) Representative images of sagittal sections stained with antibodies against the three fluorescent proteins (BFP, cyan; EGFP, green; tdTomato, red) and counterstained with NeuN antibody (white). The sagittal section near the injection sites of the FuGB2 vectors (C) shows each fluorescence-positive axon differentially innervating the S1 regions. Serial sagittal sections show the distribution of neurons positive for each type of fluorescence in the thalamus (D–E). The boxed area near the second injection site (E, left) is magnified (E, lower right) to show that the three types of projection neurons are intermingled in the thalamus. Scale bars: 1000 μm in C, D (upper left, middle, and lower), and E (left) and 200 μm in D (upper right) and E (lower right). (**F**) Confocal images of the boxed area in (E, lower right). Neurons expressed the three fluorescent proteins in a mutually exclusive manner. Scale bars: 20 μm. Adapted from Matsuyama et al. (2015).

Supplementary Table 1. The infection rates of the receptor–envelope combinations *in vitro*.

	EnvA	EnvB	EnvC	EnvE
TVA950	99.6 ± 0.041%	1.41 ± 0.32%	0.98 ± 0.040%	0.81 ± 0.52%
TVB^{S3}	0.29 ± 0.092%	97.7 ± 0.072%	2.27 ± 0.020%	1.18 ± 0.49%
TVC	0.24 ± 0.014%	0.061 ± 0.0064%	98.2 ± 0.081%	0.34 ± 0.015%
TVB^{T}	0.090 ± 0.057%	65.3 ± 0.016%	1.31 ± 0.0016%	99.6 ± 0.030%
DR-46TVB	0.27 ± 0.099%	0.51 ± 0.023%	0.89 ± 0.050%	98.8 ± 0.11%
Control	0.51 ± 0.30%	0.67 ± 0.34%	0.67 ± 0.0034%	0.58 ± 0.33%

Note: Supporting Table 1, related to Figure 3: The Env vector infection rates (the ratio of AcGFP1/mCherry double-positive cells to all AcGFP1-positive cells under each condition) for HEK 293T cells expressing each receptor. Adapted from Matsuyama et al. (2015).

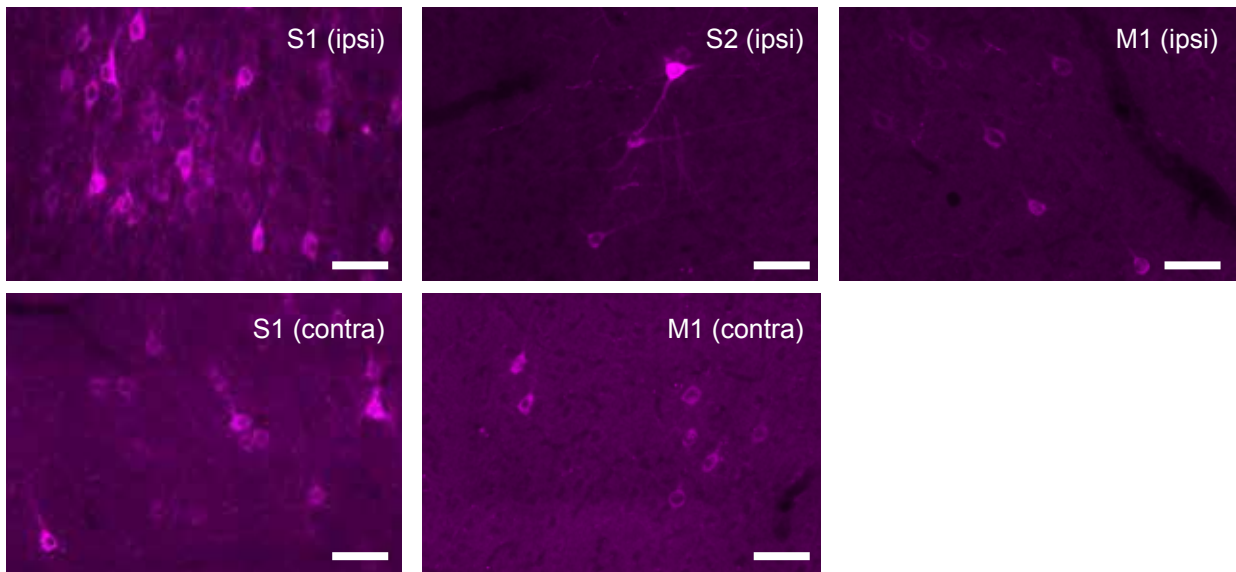Supplementary Table 2. Plasmids used for viral vector production

Viral vector	Envelope plasmid	Transfer plasmid
FuGB2-AcGFP1-P2A-TVA950	pCAGGS-FuGB2	pCL20c-CMV-AcGFP1-P2A-TVA950-WPRE
FuGB2-AcGFP1-P2A-TVB^{S3}	pCAGGS-FuGB2	pCL20c-CMV-AcGFP1-P2A-TVB^{S3}-WPRE
FuGB2-AcGFP1-P2A-DR-46TVB	pCAGGS-FuGB2	pCL20c-CMV-AcGFP1-P2A-DR-46TVB-WPRE
FuGB2-AcGFP1	pCAGGS-FuGB2	pCL20c-CMV-AcGFP1-WPRE
FuGB2-TVA950	pCAGGS-FuGB2	pCL20c-CMV-TVA950-WPRE
FuGB2-TVB^{S3}	pCAGGS-FuGB2	pCL20c-CMV-TVB^{S3}-WPRE
FuGB2-D-46TVB	pCAGGS-FuGB2	pCL20c-CMV-DR-46TVB-WPRE
EnvA-mCherry	pCB6-WTA-VCT	pCL20c-CMV-mCherry-WPRE
EnvB-mCherry	pAB7	pCL20c-CMV-mCherry-WPRE
EnvC-mCherry	pAB9	pCL20c-CMV-mCherry-WPRE
EnvA-BFP	pCB6-WTA-VCT	pCL20c-CMV-BFP-WPRE
EnvB-EGFP	pAB7	pCL20c-CMV-EGFP-WPRE
EnvC-tdTomato	pAB9	pCL20c-CMV-tdTomato-WPRE

Note: The packaging plasmids pCAG4-RTR2 and pCAG-kGP1.1R were used for all

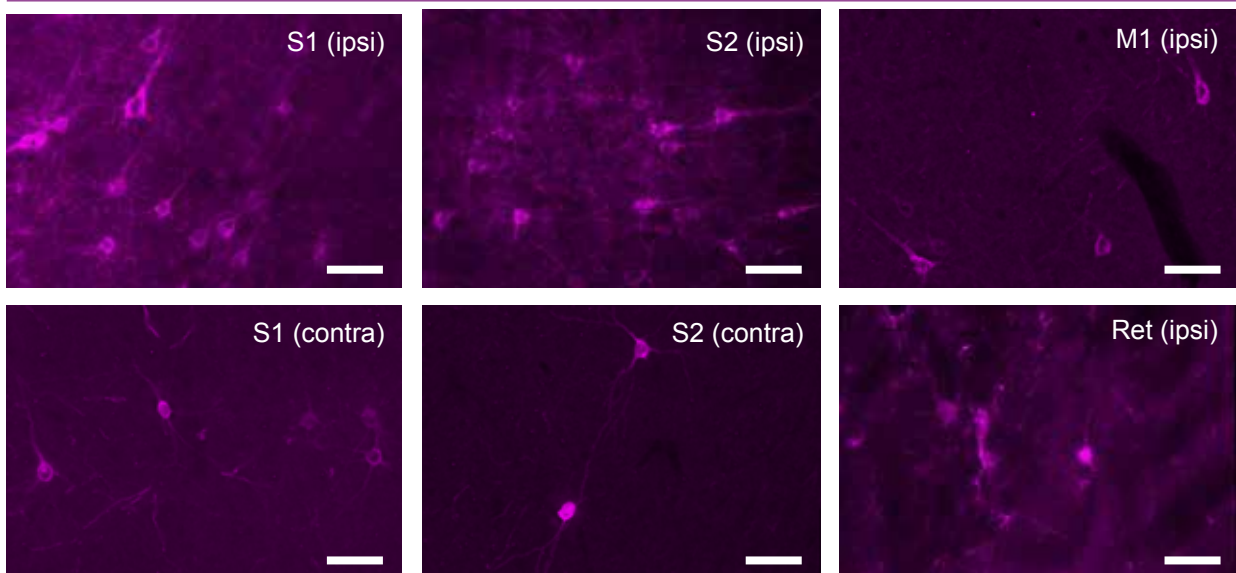viral vector production. Adapted from Matsuyama et al. (2015).
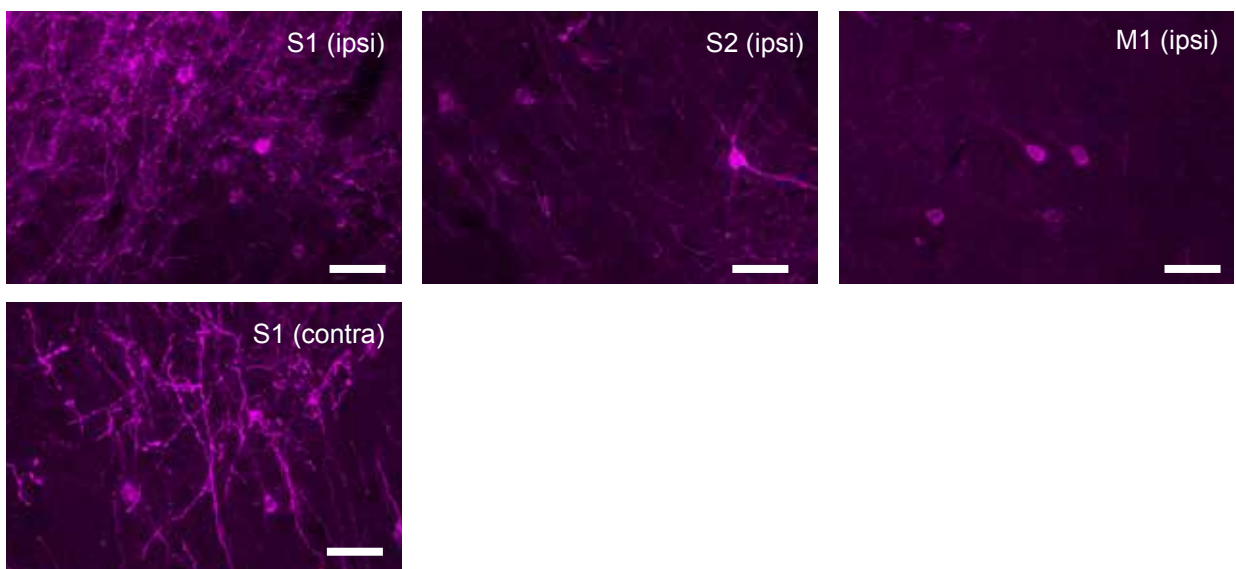
Supplementary Figure 1

A

TVA950-HA

S1 (ipsi)

S2 (ipsi)

M1 (ipsi)

S1 (contra)

M1 (contra)

B

TVB^{S3}-cMyc

S1 (ipsi)

S2 (ipsi)

M1 (ipsi)

S1 (contra)

S2 (contra)

Ret (ipsi)

C

DR-46TVB-3xFlag

S1 (ipsi)

S2 (ipsi)

M1 (ipsi)

S1 (contra)

Supplementary Figure 1. The engineered receptor expression is also observed in those brain regions projecting to the injection site of the FuGB2-receptor vectors. (**a**) Magnified images of some brain regions projecting to the injection site of FuGB2-TVA950 vector in coronal sections stained with the antibody to the HA-tag. The TVA950-positive neurons in the ipsilateral and contralateral somatosensory cortices (S1 and S2) and ipsilateral primary motor cortex (M1) are shown. Scale bars: 50 m. (**b**) Magnified images of some brain regions projecting to the injection site of FuGB2-TVBS3 in coronal sections stained with the antibody to c-Myc-tag. The TVBS3-positive neurons in the ipsilateral and contralateral S1 and S2, ipsilateral M1, and ipsilateral reticular thalamic nucleus (Ret) are shown. Scale bars: 50 m. (**c**) Magnified images of some brain regions projecting to the injection site of FuGB2-DR-46TVB in coronal sections stained with the antibody to the 3xFlag-tag. The DR-46TVB–positive neurons in the ipsilateral and contralateral S1, ipsilateral S1 and M1 are shown. Scale bars: 50 m. S1, primary somatosensory cortex; S2, secondary somatosensory cortex; M1, primary motor cortex; Ret, reticular thalamic nucleus; ipsi, ipsilateral to the FuGB2 injection site; contra, contralateral to the FuGB2 injection site. Adapted from Matsuyama et al. (2015).